Frontiers in Bioscience Landmark

Front. Biosci. (Landmark Ed) **2026**; 31(8): 52962
https://doi.org/10.31083/FBL52962

Original Research

Physiological Hypoxia as a Potent Tool for Directed Modification of the Extracellular Matrix of Multipotent Mesenchymal Stromal Cells *In Vitro*

Diana Matveeva[1,*], Aleksandra Gornostaeva[1], Elena Andreeva[1], Ludmila Buravkova[1]

[1]Cell Physiology Laboratory, Institute of Biomedical Problems of Russian Academy of Sciences, 123007 Moscow, Russia
*Correspondence: matveeva.dajana@yandex.ru (Diana Matveeva)
Academic Editor: Graham Pawelec
Submitted: 16 April 2026 Revised: 3 July 2026 Accepted: 17 July 2026 Published: 17 August 2026

Abstract

Background: Multipotent mesenchymal stromal cells (MSCs) are widely used in regenerative medicine. Their decellularized extracellular matrix (dECM) has emerged as a key bioactive substrate for tissue engineering. The properties of MSC-derived dECM depend on cell culture conditions. Physiological hypoxia mimics the native MSC milieu and represents a promising preconditioning strategy. This study aimed to evaluate the structural and mechanical properties of dECM derived from MSCs cultured under different oxygen levels and to assess the phenotype of MSCs recellularized on these matrices. **Methods:** Human adipose-derived MSCs were permanently expanded under 20% or 5% O_2 to obtain 20-dECM and 5-dECM. Matrix architecture was visualized using scanning electron microscopy and quantitative phase contrast. Stiffness of dECM was measured by atomic force microscopy. MSCs were recellularized on dECM and cultured under 20% O_2 for 72 hours. The assessment of cell morphology, cytoskeletal organization, nuclear translocation of Yes-associated protein (YAP) and transcriptional coactivator with PDZ-binding motif (TAZ), integrin expression, levels of reactive oxygen species (ROS), and cell cycle analysis were assessed using confocal microscopy and flow cytometry. **Results:** In comparison with 20-dECM, 5-dECM demonstrated significant alignment of fibrillar bundles and a 1.6-fold increase in stiffness ($p < 0.05$). Reseeded MSCs on 5-dECM have acquired a spindle-shaped, aligned morphology, whereas cells on 20-dECM displayed a rounded morphology with multiple processes. The YAP and TAZ nuclear-to-cytoplasmic ratio was significantly lower on both dECM compared with uncoated surfaces ($p < 0.0001$). Total fluorescence intensity of YAP and TAZ per cell revealed divergent patterns on 5-dECM vs 20-dECM: YAP levels were increased, whereas TAZ levels were decreased. The expression of integrin α2 and α6 was higher ($p < 0.01$), while the expression of integrin α1 and intercellular adhesion molecule 1 (ICAM-1) was lower on both dECM vs control ($p < 0.05$). Intracellular ROS levels were reduced twofold on dECM ($p < 0.01$). The proportion of MSCs in the G2/M phase and the increase in cell number were more significant on dECM compared with uncoated plastic. **Conclusions:** Hypoxia-derived dECM exhibits increased anisotropy and stiffness, promoting MSC alignment and cytoskeleton organization, integrin expression, altering the subcellular localization of YAP and TAZ and reducing ROS levels. Thus, it may represent a promising, effective bioactive scaffold for MSC expansion.

Keywords: extracellular matrix; mesenchymal stromal cells; hypoxia; surface properties

1. Introduction

Multipotent mesenchymal stromal cells (MSCs) constitute a highly promising therapeutic agent in the context of cell-based therapies and regenerative medicine [1,2,3]. Currently, cell-free MSC-derived products—soluble mediators, exosomes, and the insoluble components of the MSC secretome—and the extracellular matrix (ECM) are attracting increasing research interest [4]. The stimulatory effects of MSC-derived decellularized ECM (dECM) have been described in a number of papers. After reseeding of MSCs on such matrices, there is an enhancement in adhesion, proliferation and both directed and undirected migration [5,6,7,8,9]. Additionally, MSC-derived dECM has been shown to promote the maintenance of the naïve phenotype of progenitor cells, including hematopoietic stem and progenitor cells [10] and neuronal progenitors [11]. Furthermore, the potential for MSC differentiation in osteo-, adipo-, and chondro- directions has been shown to increase [8,12,13,14].

Preconditioning has been shown to effectively modulate the properties of MSCs and the factors they produce [15,16,17]. The priming strategy has been widely incorporated into MSC expansion protocols for clinical applications [3,18]. However, relatively few studies have specifically examined ECM alterations in preconditioned MSCs. We have reviewed the current data in a recent review article [19].

Among the various preconditioning protocols, exposure to low O_2—a physiological hypoxia characteristic of local tissue depots of MSCs—is of particular interest [20,21,22]. O_2 (5%) was used for this study, as it represents a physiologically relevant level within the MSC microenvironment and is widely employed in MSC biology research [23,24,25]. Such a hypoxic milieu has been shown to enhance the regenerative potential of MSCs, specifically

proliferation, angiogenic cytokine production, modulation of differentiation, etc. [18,26,27,28] and the production of hypoxia-inducible factor (HIF)-dependent molecules, including ECM components [29,30]. It can therefore be hypothesized that prolonged physiological hypoxia *in vitro* induces directed modifications in ECM properties. An O_2-dependent priming effect of MSCs on hypoxic dECM was demonstrated, manifested in reduced spontaneous osteoinduction and altered paracrine profile [31]. Another important area of research concerns the use of hypoxia-conditioned cells in tissue engineering constructs, such as cartilage replacement systems [28,32,33]. These findings highlight the need for further mechanistic studies of hypoxic dECM, including analyses of protein composition, topology, and mechanical properties, which are essential for the development of advanced scaffolds for tissue engineering and regenerative medicine.

The objective of this study was to investigate how physiological hypoxia (5% O_2) during MSC culture affects the structural and mechanical properties of dECM and to assess its effects on reseeded MSCs, including cell morphology, integrin expression, oxidative stress, and subcellular localization of Yes-associated protein (YAP) and transcriptional coactivator with PDZ-binding motif (TAZ).

2. Materials and Methods

2.1 Cell Culture

Human adipose tissue-derived MSCs were obtained from the Cell Physiology Laboratory (IBMP RAS) cryocollection. Written informed consent was obtained from all donors at the time of tissue collection. The use of these cells for research purposes was approved by the Medical Bioethics Commission of IBMP RAS (protocol No. 690/MSC, 11/08/25). In the experiments, the samples from 3 to 6 individual donors were used. Following thawing, MSCs were immediately split into two portions and expanded under two different O_2 conditions: first one was cultured in a CO_2 incubator under ambient air (20% O_2), while the other one was maintained in a multi-gas incubator at physiological hypoxia (5% O_2) using a calibrated gas mixture (95% N_2, 5% CO_2); both incubators from Binder GmbH (Tuttlingen, Germany). MSCs from different donors were positive for CD105, CD73 and CD90, and negative for CD34, HLA-DR and CD45 antigens, and were undergoing osteo- and adipogenic differentiation in the presence of the appropriate stimuli in the medium, satisfying minimal International Society for Cellular Therapy criteria [34]. Representative data were shown in **Supplementary Fig. 1**.

Cells were maintained in α-minimum essential medium (Gibco, Thermo Fisher Scientific, Waltham, MA, USA) supplemented with penicillin/streptomycin (100 U/mL and 100 µg/mL, respectively; PanEco, Moscow, Russia) and 10% (v/v) fetal bovine serum (Capricorn Scientific GmbH, Ebsdorfergrund, Germany). The seeding density was 3–3.5 × 10^3 cells/cm^2, with medium changes performed every 3–4 days. MSC differentiation was induced using media supplemented with appropriate stimuli. For osteogenic induction, 10^{-8} M dexamethasone, 10 mM glycerol-2-phosphate and 0.2 mM 2-phospho-L-ascorbic acid (Sigma-Aldrich, St. Louis, MO, USA) were added to α-MEM. Osteogenic differentiation was verified after staining of the mineralized matrix components with Alizarin red (Merck Millipore, Burlington, MA, USA). For adipogenic induction, 0.5 mM isobutylmethylxanthine, 1 µM dexamethasone, 10 µg/mL insulin, and 200 µM indomethacin (Sigma-Aldrich, St. Louis, MO, USA) were added to the culture medium. Adipocyte differentiation was confirmed with Oil Red O staining of intracellular lipid droplets (Merck Millipore, Burlington, MA, USA).

Experiments were conducted using MSCs at passages 2 to 5. For all cell handling procedures, the culture medium was pre-equilibrated in the hypoxic CO_2 incubator to ensure consistent O_2 levels throughout manipulations.

In order to obtain samples of ECM, MSCs were seeded at a density of 7.5 × 10^3 cells/cm^2 and cultured for 14 days under 20% or 5% O_2. When cell layers had reached approximately 80% confluence, 50 µg/mL of sodium 2-phospho-L-ascorbate (Fluka, Sigma-Aldrich, Buchs, Switzerland) was added to the culture medium to stimulate the production of ECM.

2.2 Decellularization

In the present study, the term "dECM" refers to ECM derived from MSCs *in vitro* following the removal of cellular components using detergents. To remove cellular components, the mixture of 0.5% Triton X-100 in phosphate-buffered saline (PBS) and 20 mM NH_4OH (PanEco, Moscow, Russia) was added to MSC monolayers and kept for 5 min at 37 °C. To remove nucleic acid residues, ECM samples were treated with 50 U/mL DNase (SciStore, Moscow, Russia) for 30 min at 37 °C. Decellularization of ECM samples was performed under ambient O_2. To control membrane component and DNA contamination, dECM preparations were stained using CellTracker Dil-dye (5 µM, Ex/Em = 553/570 nm, Thermo Fisher Scientific, Waltham, MA, USA) and propidium iodide (PI) (50 µg/mL, Ex/Em = 535/617 nm, Molecular Probes, Thermo Fisher Scientific, Waltham, MA, USA), respectively. Representative microphotographs are shown in **Supplementary Fig. 2**.

2.3 Scanning Electron Microscopy

Decellularized ECM samples were washed twice with PBS, pH 7.2, and fixed in a mixture of 2.5% glutaraldehyde and 2% paraformaldehyde (Merck KGaA, Darmstadt, Germany) in PBS for 12 hours at 4 °C. Subsequently, the samples underwent dehydration through ethanol solutions with rising alcohol concentrations, ranging from 30% to 100%. Following this, the ethanol was substituted with high-purity acetone (Himmed, Moscow, Russia). The sam-

ples were then dried at the critical point using a HCP-2 critical point dryer (Hitachi High-Technologies Corporation, Tokyo, Japan). At the final step, the ECM structures were coated with a 15-nanometer-thick conductive layer of gold-palladium alloy by vacuum sputtering. The samples were examined using a scanning electron microscope JSM-6380LA (JEOL Ltd., Tokyo, Japan).

2.4 Atomic Force Microscopy

Surface images were acquired using an NT-MDT Solver P47 microscope (NT-MDT Spectrum Instruments, Moscow, Russia) with an NSG01 TiN cantilever operating at a scanning resonance frequency of 100 to 200 kHz. Atomic force microscopy (AFM) image processing was performed using Image Analysis software version 3.5.4.

The dECM was mechanically characterized using AFM (NTEGRA NEXT II, NT-MDT Spectrum Instruments, Moscow, Russia). Measurements were performed in contact mode in PBS using colloidal cantilevers with a 6.5 µm diameter sphere (TipsNano OÜ, Tallinn, Estonia) and a spring constant of 0.08–0.15 N/m. Force indentation curves were acquired on glass coverslips for calibration. For each sample, 80–140 force curves were collected with a maximum indentation depth of 500 nm. The substrate stiffness (Ks) was calculated as an effective spring constant according to Hooke's law: $Ks = F/\delta$, where F is the applied force (N) and δ is the indentation depth (m). The reported values (pN/nm) represent the spring constant, not an elastic modulus. This choice was determined by the peculiarities of MSC-derived dECM. The thin, fibrillar, anisotropic structure of ECM does not satisfy Hertzian assumptions (homogeneity, isotropy, infinite thickness). Hooke's law provides a direct, assumption-free metric (spring constant, pN/nm) suitable for relative comparative analysis between samples.

2.5 Quantitative Phase Imaging With Digital Holographic Microscopy (Holotomography)

For three-dimensional visualization of unprocessed ECM structures, a Tomocube HT-X1 microscope (Tomocube Inc., Daejeon, Republic of Korea) equipped with a high numerical aperture (NA 1.2) immersion objective was utilized. dECM samples were placed in glass-bottom Petri dishes and positioned on the microscope stage. Imaging was conducted in quantitative phase imaging mode, which enables the detection of phase shifts in light passing through the sample without the need for fixation or staining. This method allowed for accurate visualization of the ECM's native architecture. Visualization was performed using a 532 nm wavelength laser in a layer-by-layer fashion, acquiring 60 optical sections across a total depth of 600 µm. For the final analysis, 6 consecutive sections corresponding to the actual thickness of the dECM were selected.

2.6 Recellularization of MSCs on dECM

Reseeding experiments were carried out under standard laboratory conditions 20% O_2 to exclude the influence of reduced O_2 level on recellularized cells. MSCs (primary density of 3×10^3 cells/cm^2) were cultured for 72 hours on different substrates. The MSCs' number was calculated in a Neubauer Counting Chamber (Marienfeld Superior GmbH & Co. KG, Lauda-Königshofen, Germany) before reseeding (day 0) and after 72 hours of cultivation. Culture dishes with MSC-derived dECM obtained under 20% or 5% O_2 (20-dECM and 5-dECM, respectively) were directly used for recellularization experiments. Uncoated tissue culture plastic or glass coverslips (Corning Inc., Corning, NY, USA) were used as surfaces of comparison (controls). The cell morphology was evaluated using Eclipse Ti-U phase contrast microscopy (Nikon Corporation, Tokyo, Japan).

2.7 Immunocytochemistry

Recellularized MSCs were washed twice with PBS and fixed in a mixture of 4% w/v paraformaldehyde and 0.2% v/v Triton X-100 in PBS at 37 °C for 15 minutes. Nonspecific antibody binding was blocked with 3% bovine serum albumin (Sigma-Aldrich, St. Louis, MO, USA) for 30 minutes at room temperature.

Rhodamine-labeled phalloidin (1:50, Molecular Probes, USA) was used to detect F-actin. Paxillin in focal adhesions and transcriptional activators (YAP, TAZ) were detected by indirect immunocytochemistry. Anti-paxillin primary rabbit antibody (1:100, Cat. No. sc-5574 Santa Cruz Biotechnology, Dallas, TX, USA), anti-YAP primary rabbit antibody (1:100, Cat. No. E-AB-62344, Elabscience Biotechnology Inc., Wuhan, China), anti-TAZ primary mouse antibody (1:50, Cat. No. sc-518026, Santa Cruz Biotechnology, Dallas, TX, USA), and secondary goat anti-rabbit IgG antibody labeled with Elab Fluor-488 (1:100, Cat. No. E-AB-1055, Elabscience Biotechnology Inc., Wuhan, China), Elab Fluor-647 (1:100, Cat. No. E-AB-1075, Elabscience Biotechnology Inc., Wuhan, China) and goat anti-mouse IgG antibody labeled with Elab Fluor-488 (1:100, Cat. No. E-AB-1056, Elabscience Biotechnology Inc., Wuhan, China) were used. The nuclei were counterstained with DAPI in mounting medium (Beijing Solarbio Science & Technology Co., Ltd., Beijing, China). A laser-scanning confocal microscope LSM-780 (Carl Zeiss Microscopy GmbH, Jena, Germany) was used for microscopic analysis.

2.8 Quantitative Image Analysis

Confocal image processing was conducted in CellProfiler software v.4.2.6 (Broad Institute, Cambridge, MA, USA). For each experimental condition, more than 1000 cells were analyzed, derived from three independent experiments. Nuclei were segmented from the DAPI channel using its IdentifyPrimaryObjects module. Based on

the identified nuclei, whole-cell segmentation was performed on 488-channel (fluorescence of TAZ) using the IdentifySecondaryObjects module, generating regions of interest (ROIs) corresponding to individual cells. The mean fluorescence intensities (MFI) of TAZ (488-channel) and YAP (647-channel) were measured within these ROIs. After segmenting nuclei and cells, the cytoplasmic ROI was obtained by subtracting the nuclear ROI from the whole-cell ROI. The mean fluorescence intensity was measured separately within the nuclear and cytoplasmic regions. Nuclear translocation was assessed by calculating the nuclear-to-cytoplasmic (N/C) fluorescence intensity ratio. The N/C ratio was calculated as: N/C Ratio = MFI_nucleus/MFI_cytoplasm. An increase in the N/C ratio was interpreted as enhanced translocation into the nucleus.

2.9 Flow Cytometry

The MSC surface antigens were analyzed by flow cytometry using the following monoclonal antibodies: involved in cell-to-cell (CD54-PE (ICAM-1)), and cell–ECM interactions: CD49a-PE (integrin α1), CD49b-FITC (integrin α2), CD49c-PE (integrin α3), CD49d-FITC (integrin α4), CD49e-PE (integrin α5), CD49f-FITC (integrin α6), CD29-APC (integrin β1). For MSC immunophenotype identification, CD90-APC, CD73-PE, and CD105-PE were used as positive markers and HLA-DR-FITC, CD45-FITC, and CD34-FITC as negative markers. The IgG-FITC, IgG-PE, and IgG-APC were used as negative controls (all reagents from BD Biosciences, San Jose, CA, USA). Data were collected on a CytoFLEX (Beckman Coulter Life Sciences, Indianapolis, IN, USA) flow cytometer using the CytExpert 2.5.0.77 (Beckman Coulter Life Sciences, Indianapolis, IN, USA) software. The obtained data were processed using Kaluza Analysis version 2.3. (Beckman Coulter Life Sciences, Indianapolis, IN, USA). The gating strategy was as follows. First, the target cell population was identified on the side scatter/forward scatter (SSC/FSC) plot based on the appropriate cell size and side scatter characteristics. Next, only singlet cells were selected from this population, while doublets were excluded using the FSC-A versus FSC-H plot. Histograms of cellular fluorescence were then generated based on the singlet gate.

A PI-based test was performed to analyze the cell cycle. Cells were fixed with cold 70% ethanol within 30 min at 4 °C in the dark. Then, cells were washed by centrifugation with PBS and then PBS containing 25 µg/mL RNase A (Sigma, USA) and 50 µg/mL PI (Molecular Probes, USA) was added to the samples. The fluorescence intensity proportional to the amount of DNA in the cell was measured using flow cytometry. The data are presented as the percentage of cells in the G2/M phase of the cell cycle, as an indicator of cells preparing for division and undergoing mitosis.

Fluorescent probes were used to analyze mitochondrial compartment and oxidative stress levels of cells. MitoTracker Green FM (Mitogreen) (Molecular Probes, Thermo Fisher Scientific, Waltham, MA, USA), which determines the total volume of mitochondria, and potential-dependent tracker JC-1 (Life Technologies, Thermo Fisher Scientific, Waltham, MA, USA) were used to characterize the functional activity of mitochondria according to the manufacturer's instructions. Detection of ROS was performed using CM-H_2DCFDA (Life Technologies, Thermo Fisher Scientific, Waltham, MA, USA) according to the manufacturer's instructions. CytoFLEX flow cytometer was used to analyze the fluorescence.

2.10 Reverse Transcription Quantitative Polymerase Chain Reaction (RT-qPCR) Analysis

Total RNA was extracted from cultured MSCs using phenol-chloroform extraction with the ExtractRNA kit (Evrogen, Moscow, Russia). To eliminate residual genomic DNA, each nucleic acid sample was treated with DNase I (Invitrogen, Thermo Fisher Scientific, Waltham, MA, USA). RNA purification was performed using spin columns following the manufacturer's instructions (CleanRNA Standard kit, Evrogen, Moscow, Russia). The purity of all RNA samples was assessed using a Nanodrop 2000 spectrophotometer (Thermo Fisher Scientific, Waltham, MA, USA).

A reverse transcription reaction was performed using an MMLV RT kit (Eurogen, Moscow, Russia) according to the manufacturer's instructions. Subsequently, the resulting cDNA was utilized for quantitative PCR (qPCR) on an Mx3000P instrument (Agilent Technologies, Santa Clara, CA, USA) with a commercially available qPCRmix-HS SYBR dye (Eurogen, Moscow, Russia). A Stratagene 3000 amplifier (Agilent Technologies, Santa Clara, CA, USA) was utilized for this purpose.

Appropriate commercial primers (QIAGEN GmbH, Hilden, Germany) were used to analyze the expression of genes encoding ECM-associated proteins (type I collagen (*COL1A1*), prolyl 4-hydroxylase (*P4HA1*), procollagen-lysine, 2-oxoglutarate 5-dioxygenase 2 (*PLOD2*), matrix metallopeptidase 1 (*MMP1*), and plasminogen activator, urokinase (*PLAU*)); cytoskeletal proteins, including actin beta (*ACTB*) and tubulin beta class I (*TUBB*); and actin cytoskeleton regulators, including Ras homolog family member A (*RHOA*) and Rho-associated coiled-coil containing protein kinase 1 (*ROCK1*). Ribosomal protein lateral stalk subunit P0 (*RPLP0*) and hypoxanthine phosphoribosyltransferase 1 (*HPRT1*) (QIAGEN GmbH, Hilden, Germany) were used as housekeeping genes.

2.11 Statistical Analysis

Statistical analysis was performed using GraphPad Prism 9 (GraphPad Software, LLC, USA, San Diego, CA). The experiments were carried out on primary MSC cultures, each derived from a single adipose tissue sample of different donors. In each experiment, MSCs from 3 to 6 samples were taken, as indicated in the figure legends. The data

are presented as mean ± standard deviation (M ± SD). The Mann–Whitney test was used for two-group comparisons when data were not normally distributed. For multiple-group comparisons, one-way ANOVA with Tukey's post hoc test was applied for normally distributed data, while the Kruskal–Wallis test with Dunn's post hoc test was used for non-normally distributed data; $p < 0.05$ was considered statistically significant. The choice of statistical test was based on the normality assessment with the Shapiro–Wilk normality test.

3. Results

3.1 The Peculiarities of ECM Produced by MSCs at Different O_2 Levels

To determine how different O_2 levels affect dECM formation by MSCs, we first analyzed the transcription of genes encoding ECM-related proteins involved in collagen fibril assembly and cross-linking. As shown in Fig. 1A, the expression of the major structural component, *COL1A1*, as well as key enzymes involved in collagen biosynthesis, stabilization, and cross-linking—*P4HA1* and *PLOD2*—was upregulated.

Next, the structural and mechanical properties of dECM samples derived from MSCs cultured under 20% or 5% O_2 were analyzed (Fig. 1B–E). Hereafter, the terms 20-dECM and 5-dECM are used to denote ECM derived from MSCs cultured under 20% or 5% O_2, respectively.

Scanning electron microscopy demonstrated that 20-dECM exhibited membrane-like structures composed of curved fibrils without a defined orientation. In contrast, under hypoxic conditions (5% O_2), the dECM consisted of thick, highly aligned fibrillar bundles (Fig. 1B). Layer-by-layer quantitative phase imaging enabled detailed study of the morphology, density, and distribution of fibers within dECM samples across a total thickness of approximately 60 μm (based on 6 selected optical sections) (Fig. 1C).

Finally, the ECM surface was visualized using AFM, and its mechanical properties were quantified (Fig. 1D). AFM confirmed the differences in fibrillary organization and revealed a 1.6-fold increase in stiffness index of 5-dECM compared with 20-dECM (Fig. 1E).

3.2 The Recellularization of dECM Derived From MSCs Under Different O_2 Levels in Milieu

To evaluate the effects of the topology and mechanical properties of 20-dECM and 5-dECM on cell behavior, MSCs were reseeded on the dECM samples.

The morphology of MSCs reseeded on different substrates was assessed after 72 hours (see Fig. 2A, left panel). The 72-hour time point was selected because it allowed MSCs to fully adhere and establish focal adhesions without reaching confluence, thereby enabling clear visualization of substrate-dependent morphological differences while minimizing the confounding effects of newly synthesized cell-derived ECM deposition. On uncoated surfaces, MSCs were large, flattened, and randomly distributed. Conversely, MSCs on dECM exhibited distinct substrate-dependent morphologies. On 20-dECM, cells were uniformly distributed, displayed a rounded morphology, and possessed multiple cellular processes. On 5-dECM, cells adopted a spindle-shaped morphology and were distributed unevenly, forming bundle-like structures.

Analysis of cytoskeleton-associated genes in MSCs reseeded on 20-dECM revealed downregulation of *ROCK1*, which encodes ROCK-1 kinase involved in F-actin stabilization and contractility (Fig. 2B). No significant changes were observed in the expression of its upstream regulator, *RHOA*. On 5-dECM, *ROCK1* expression showed a decreasing trend. No differences were detected in the expression of genes encoding cytoskeletal proteins, including *ACTB* and *TUBB*. In addition, MSCs cultured on dECM exhibited significant upregulation of the protease-encoding genes *MMP1* and *PLAU* compared with the control group (Fig. 2B).

3.3 YAP and TAZ Nucleo-Cytoplasmic Shuttling

Given the observed differences in dECM properties under 20% and 5% O_2, we further evaluated whether YAP and TAZ localization correlated with the functional behavior of recellularized MSCs.

The N/C distribution of YAP and TAZ was analyzed by confocal microscopy (Fig. 3A) followed by quantitative image analysis. The TAZ N/C ratio was found to be significantly higher in MSCs cultured on uncoated substrates compared with dECM (Fig. 3B, left panel), being 1.9-fold higher than on 20-dECM and 2.3-fold higher than on 5-dECM. In addition, the TAZ N/C ratio was significantly higher on 20-dECM versus 5-dECM. A comprehensive analysis of the total fluorescence intensity per cell detected that the overall levels of TAZ were 7% higher in MSCs on 20-dECM compared with those on 5-dECM.

Similarly, the YAP N/C ratio was decreased on both dECM substrates in comparison with the uncoated glass control (Fig. 3B, right panel), with a 17% reduction on 20-dECM and 14% on 5-dECM. In contrast to TAZ, total YAP fluorescence intensity per cell was higher on 5-dECM compared with 20-dECM.

3.4 Expression of Adhesion Molecules and Activity of Intracellular Compartments in Recellularized MSCs

To characterize MSC–ECM interaction, the adhesion-related molecules, including integrin α- and β-subunits and ICAM-1, were identified on MSCs (Fig. 4). The expression levels of integrin α1 and ICAM-1 in MSCs reseeded on dECM were found to be reduced in comparison with the uncoated surface. The expression of integrins α3, α4, α5, and β1 remained unchanged, whereas the expression of α2 and α6 was increased. No significant differences in the expression of adhesion molecules were observed between MSCs cultured on 20- and 5-dECM.

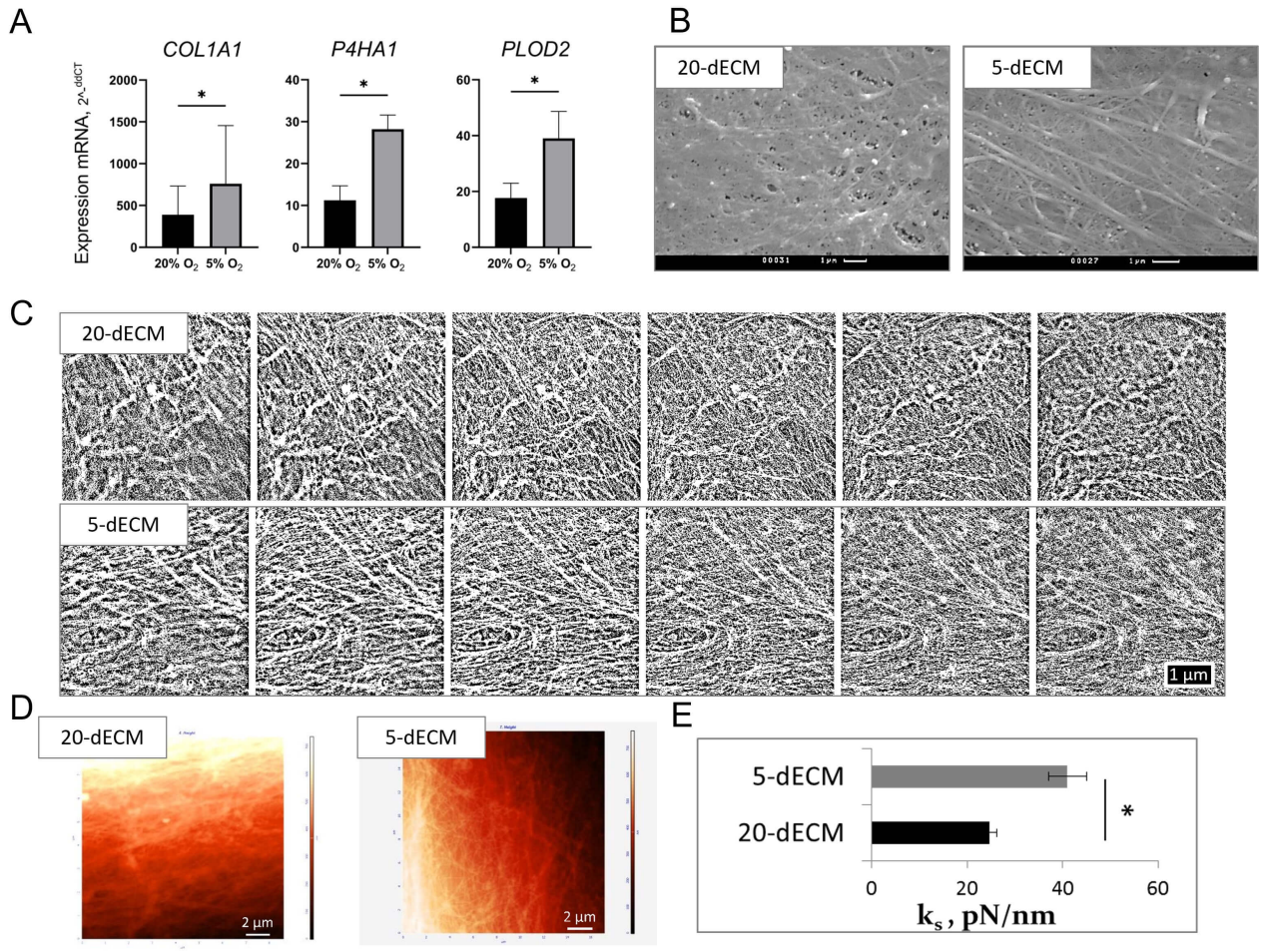

Fig. 1. Characterization of ECM derived from MSCs under 20% or 5% O_2. (A) Relative levels of genes encoding collagen I type (*COL1A1*), prolyl 4-hydroxylase (*P4HA1*), and procollagen-lysine, 2-oxoglutarate 5-dioxygenase 2 (*PLOD2*). The data were normalized to housekeeping genes (hypoxanthine phosphoribosyltransferase 1 (*HPRT1*) and ribosomal protein lateral stalk subunit P0 (*RPLP0*)) and are presented as mean ± SD (n = 3), *$p < 0.05$ (Mann–Whitney test). (B) Surface texture of MSC-derived dECM was visualized with scanning electron microscopy (JSM-6380LA). Representative images. Scale bar: 1 µm. (C) Quantitative phase imaging of dECM using Tomocube HT-X1. Serial optical sections (Z-stack) were acquired through the thickness of the sample with a 10 µm step size. Representative sections are shown. Scale bar: 1 µm. (D) Atomic force microscopy visualization of 20-dECM and 5-dECM. Representative height topography images. Scale bar: 2 µm. (E) Stiffness (Ks, pN/nm) of 20-dECM and 5-dECM measured in liquid mode using a colloidal cantilever with a 6.5 µm diameter sphere. Data are presented as mean ± SEM (n = 3; N = 80–140), *$p < 0.05$ (Mann–Whitney test). 20-dECM and 5-dECM refer to the ECM derived from MSCs at 20% or 5% O_2, respectively. ECM, extracellular matrix; MSCs, mesenchymal stromal cells; dECM, decellularized extracellular matrix; HPRT1, hypoxanthine phosphoribosyltransferase 1; RPLP0, ribosomal protein lateral stalk subunit P0.

The activity of intracellular compartments was assessed using fluorescent trackers. Representative images of mitochondrial staining, JC-1 fluorescence shifts and ROS levels are shown in Fig. 5A. Quantitative flow cytometric analysis is presented in Fig. 5B. No statistically significant differences in mitochondrial mass or mitochondrial transmembrane potential were observed in MSCs cultured on different substrates. However, intracellular ROS levels were approximately twofold lower in MSCs cultured on 20-dECM and 5-dECM compared with the uncoated cover glass control.

Cell cycle analysis has demonstrated a twofold increase in the proportion of MSCs in the G2/M phase on both types of dECM compared with the control ($p < 0.001$) (Fig. 5C). These findings were further supported by cell counting data obtained on day 0 (prior to seeding) and following 72 hours in culture. After 72 hours, the number of MSCs showed a slight but statistically significant increase. MSC numbers on uncoated plastic were lower than on dECM produced under both 20% O_2 and 5% O_2 ($p < 0.05$) (Fig. 5D).

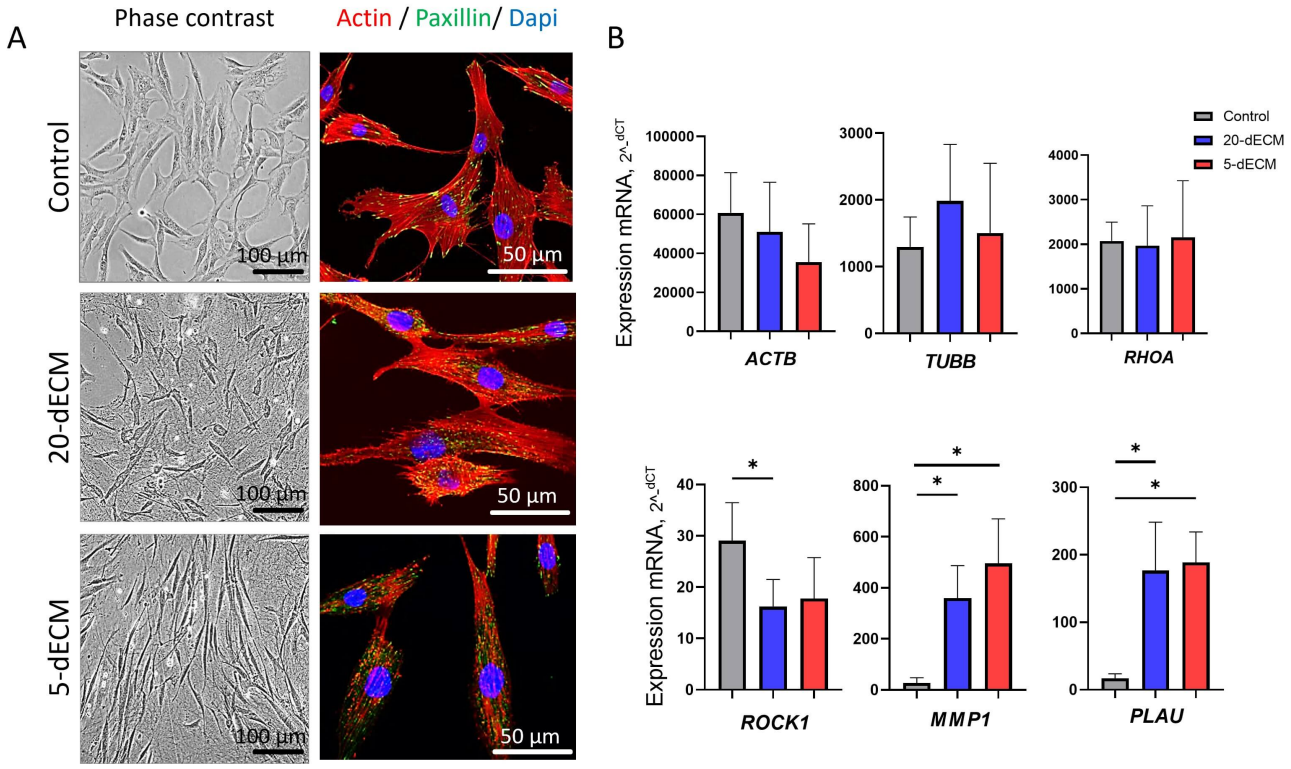

Fig. 2. Morphology and adhesion of recellularized MSCs on different surfaces. (A) The phenotype of reseeded MSCs. Left panel: phase-contrast microscopy (Nikon Eclipse TiU). Scale bar: 100 µm. Right panel: immunocytochemical staining of F-actin (red) and paxillin (green). Confocal laser scanning microscopy (Zeiss LSM 780). Scale bar: 50 µm. Nuclei were counterstained with DAPI (blue). (B) Relative gene expression of cytoskeletal proteins (*ACTB*, *TUBB*), regulators of the actin cytoskeleton (*RHOA*, *ROCK1*), and proteases (*MMP1*, *PLAU*). Quantitative reverse transcription PCR (RT-qPCR). Data were normalized to a reference gene (*HPRT1*, *RPLP0*) and are presented as the mean ± SD (n = 3). **p* < 0.05 (Kruskal–Wallis test with Dunn's post hoc test). 20-dECM and 5-dECM refer to the ECM derived from MSCs at 20% or 5% O_2, respectively; Control—uncoated culture ware. *ACTB*, actin beta; *TUBB*, tubulin beta class I; *RHOA*, ras homolog family member A; *ROCK1*, Rho-associated coiled-coil containing protein kinase 1; *MMP1*, matrix metallopeptidase 1; *PLAU*, plasminogen activator, urokinase; *RPLP0*, ribosomal protein lateral stalk subunit P0; *HPRT1*, hypoxanthine phosphoribosyltransferase 1.

4. Discussion

Native tissue-derived dECM is being extensively integrated into a wide range of applications for tissue engineering and regenerative medicine as a source of biological scaffolds [35,36]. *In vitro* cell-derived ECM presents promising opportunities for structural, molecular, and biophysical analysis of how microenvironmental cues influence ECM properties [37]. The changes in O_2 levels have been shown to modulate ECM, affecting both its composition and biophysical properties [33,38,39]. As we have demonstrated recently, physiological hypoxia, as a key physical parameter of the MSC niche, modulates the MSC-derived matrisome in an HIF-3α-dependent manner. We also demonstrated that hypoxia-derived dECM were able to maintain hypoxic competence. After recellularization, MSCs on hypoxic dECM demonstrated attenuated osteocommitment, but increased susceptibility to osteoinduction [31,40]. The present study aimed to examine the mechanical properties of dECM derived by MSCs under permanent physiological hypoxia and the phenotypic and functional responses of reseeded MSCs.

Stromal lineage cells, including MSCs, are known to produce a sufficient amount of ECM *in vitro* [41]. Previously, fibroblast-derived ECM fibrils cultured under ambient oxygen conditions were shown to be evenly distributed and to lack a defined orientation [37]. Pronounced structural anisotropy, characterized by a significant increase in the alignment of ECM fibrils synthesized by hypoxic MSCs, was described in our recent study [31].

In the present study, we have employed a high-tech quantitative phase contrast imaging approach for visualization of the native structure of ECM without sample processing. Layer-by-layer scanning revealed that the packing pattern was preserved throughout the ECM layer, with the fibrils within 5-dECM adopting an oriented structure. It has been established that ECM alignment is associated with the activity of regulatory cross-linking enzymes. Hypoxia-dependent upregulation of enzymes in-

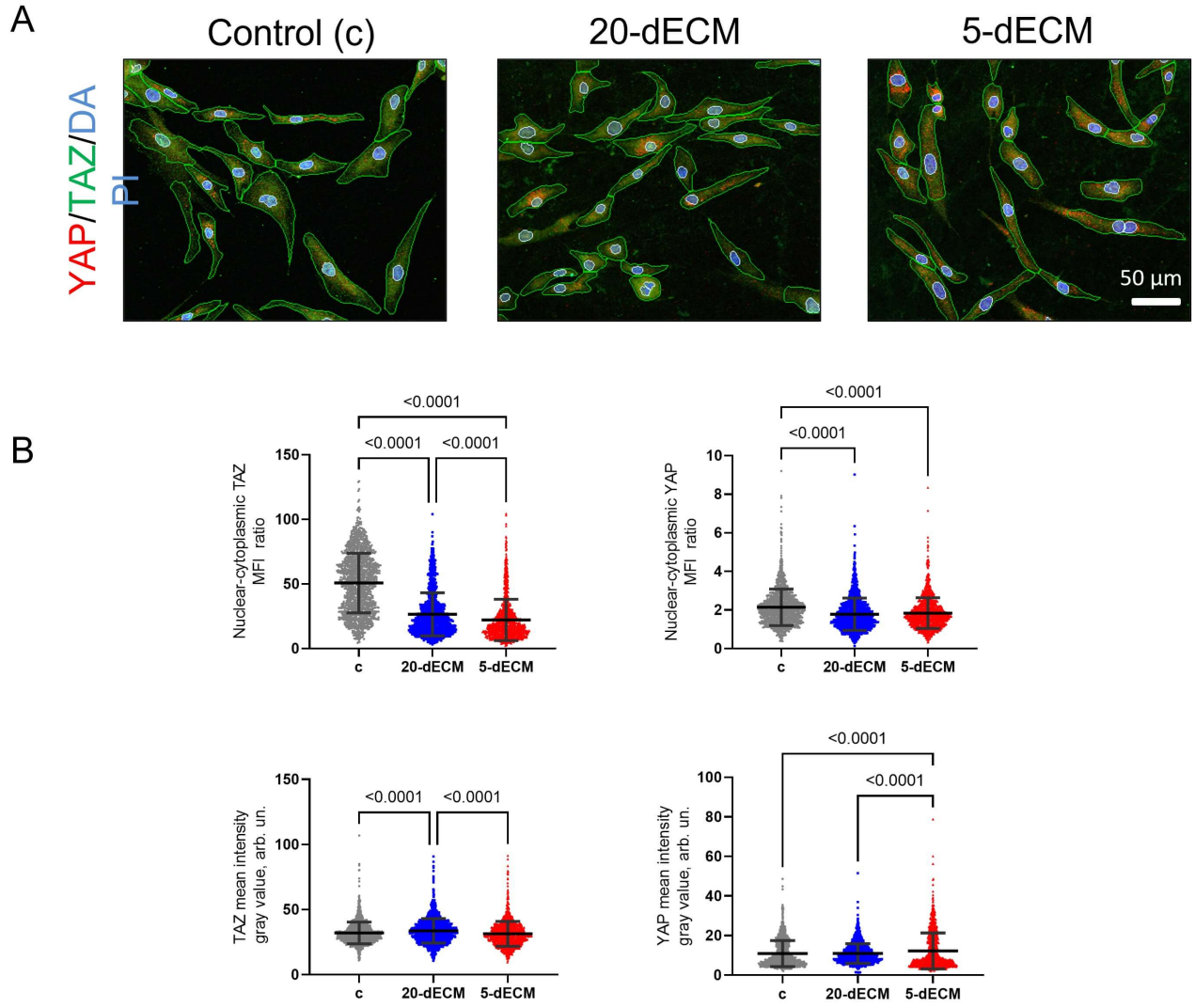

Fig. 3. Nuclear–cytoplasmic localization of YAP and TAZ in MSCs recellularized on different substrates. (A) Representative confocal images of MSCs immunostained for YAP (red) and TAZ (green). Nuclei were counterstained with DAPI (blue). Scale bar: 50 µm. Nuclear outlines (dashed white lines) and cytoplasmic outlines (dashed green lines) were delineated using CellProfiler. (B) Quantitative analysis of confocal images. For each substrate, the upper panels show the nuclear-to-cytoplasmic (N/C) ratio of MFI for TAZ (left) and YAP (right). The lower panels show the total fluorescence intensity per cell for TAZ and YAP, respectively. Data are presented as mean ± SD (n = 3 biological replicates; N = 1300 cells analyzed per condition). Statistical significance was assessed using the Kruskal–Wallis test with Dunn's post hoc test. 20-dECM and 5-dECM refer to the ECM derived from MSCs at 20% or 5% O_2, respectively; Control (c)—uncoated cover glass. YAP, Yes-associated protein; TAZ, transcriptional coactivator with PDZ-binding motif; MFI, mean fluorescence intensities.

volved in post-translational modification may contribute to fibril alignment and increased ECM stiffness [30,42,43,44]. In the present study, *P4HA1* and *PLOD2*, encoding enzymes involved in three-dimensional folding and mechanical stability of collagen fibrils, were upregulated in MSCs at 5% O_2. A key mechanistic question is why this upregulation leads to the formation of highly aligned fibrillar bundles rather than simply increased ECM deposition. The available literature suggests that hypoxia-inducible factor 1 (HIF-1) not only increases the expression of prolyl and lysyl hydroxylases (P4HA, PLOD) but also stimulates the production of lysyl oxidases (LOX) and LOX-like enzymes (LOXL2, LOXL4) [30,42,43,44]. These enzymes catalyze the formation of covalent cross-links between adjacent collagen fibrils, which promote fibril alignment and increase matrix stiffness. Consistent with this, our previously published data [40] demonstrated that MSCs cultured under 5% O_2 exhibit upregulation of LOXL4 without enhancement of ECM deposition. This finding supports the hypothesis that the aligned structure of 5-dECM described here arises, at

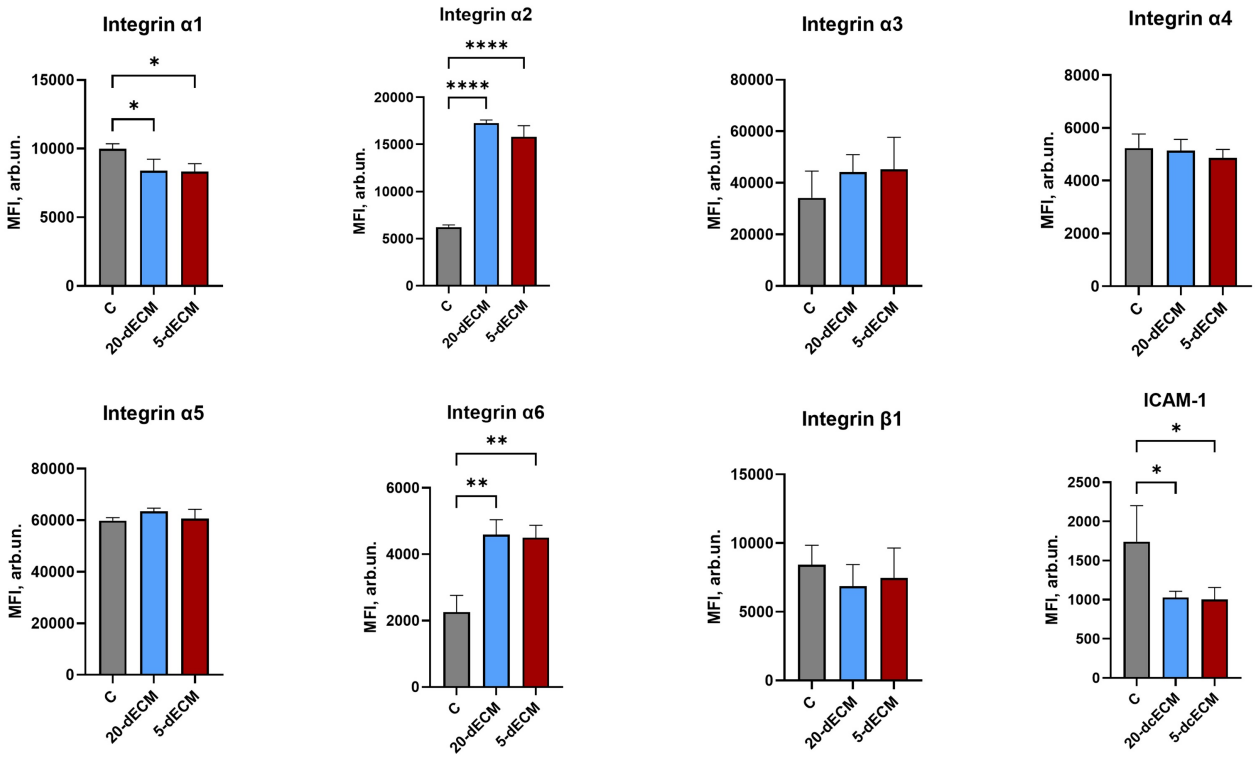

Fig. 4. Expression of adhesion molecules on MSCs after 72 hours of recellularization. Bar graphs show the MFI measured by flow cytometry (CytoFLEX). Substrates: c (control, uncoated plastic), 20-dECM, and 5-dECM. Data are presented as mean ± SD (n = 3), *p < 0.05, **p < 0.01, ****p < 0.0001 (one-way ANOVA with Tukey's post hoc test). 20-dECM and 5-dECM refer to the ECM derived from MSCs at 20% or 5% O_2, respectively; C—control, uncoated plastic ware.

least in part, from increased cross-linking of collagen fibrils due to hypoxia-dependent ECM modification. These data further support the concept that altering a single parameter (O_2 level) to physiological levels can significantly modulate MSC-derived ECM properties.

When cultured on substrates with varying topographies, cells exhibit a strong capacity to sense specific substrate patterns and respond accordingly [45]. To characterize the impact of matrix topology, MSCs were reseeded on 20-dECM and 5-dECM. After 72 hours, MSCs had not yet reached the density of a monolayer; thus, their shapes could be examined. Hypoxia-derived dECM governed the cell orientation through aligned fibrillar architecture, while on 20-dECM, cells exhibited more rounded bodies and multiple processes, suggesting a probing of the direction of movement. Similar findings were reported by Wang et al. [46], in which structuring and alignment of fibronectin fibrils led to an acquisition of bipolar cellular shapes and a decrease in the number of cell processes. It was demonstrated that aligned fibrils could govern the orientation of neurite growth [47] and vascular branching [48], stimulate osteogenesis [49] and chondrogenesis [50] in explants, and augment fibroblast migration [46]. Consequently, an increased anisotropy of 5-dECM indicates a more directionally organized matrix, potentially guiding cell alignment and migration. These properties may be of interest for tissue engineering, but require further confirmation through functional tests.

Cell spreading is accompanied by the reorganization of the actin cytoskeleton and the formation of integrin-enriched focal adhesion sites, which are responsible for signal transduction between the extracellular matrix and cells [51]. Here we described the specific features of the actin cytoskeleton in MSCs on dECM and uncoated culture plastic, which may be attributed to their stiffness, as well as to the number of adhesion sites. The high stiffness of the plastic ware restricts the reorganization of the cytoskeleton, thereby promoting the formation of substantial F-actin stress fibers, while the constrained availability of adhesion molecules induces the formation of large and sparse focal adhesion plaques [52]. On softer and multicomponent dECM, MSCs acquire a more functional morphology with a uniform distribution of the paxillin-containing focal adhesion sites appearing as small clusters along the entire cell body [46]. Other focal adhesion components, including integrin, were also differently presented on MSCs reseeded on dECM and uncoated plastic. On dECM, the increase in surface expression of α2 and α6 integrin, and the decrease of α1 integrin demonstrated the impact of substrate properties on integrin activation and clustering. Previous studies

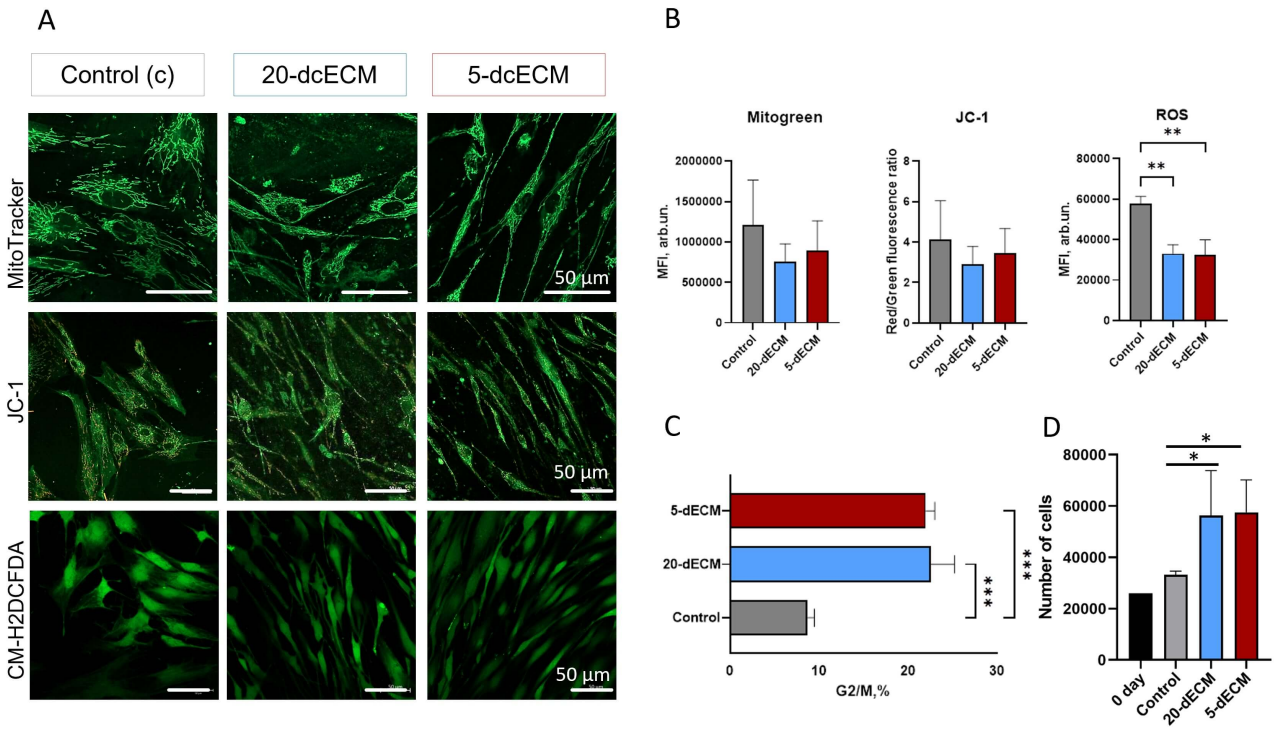

Fig. 5. The activity of intracellular compartments and cell cycle analysis of MSCs reseeded on different substrates. (A) Live imaging of MitoTracker Green (mitochondrial mass), JC-1 (membrane potential, red/green ratio), and CM-H_2DCFDA (ROS). Confocal microscopy (Zeiss LSM 780). Scale bar: 50 µm. Representative images are shown. (B) Quantitative flow cytometry (CytoFLEX) of Mitogreen, JC-1 (red/green ratio), and CM-H_2DCFDA fluorescence. (C) Percentage of cells in the G2/M phase measured by flow cytometry (CytoFLEX). (D) The MSCs' number was calculated in a Neubauer Counting Chamber before reseeding (day 0) and after 72 hours in culture (B–D). Data are shown as mean ± SD (n = 3), *$p < 0.05$, **$p < 0.01$, ***$p < 0.001$ (Kruskal–Wallis test with Dunn's post hoc test). 20-dECM and 5-dECM refer to the ECM derived from MSCs at 20% or 5% O_2, respectively; Control—uncoated cover glass.

have shown that the overexpression of integrin α1, which binds non-specifically to the surface, was observed on rigid plastic [53]. In contrast, on collagen- and laminin-enriched matrices, more specific integrins, such as α2 [53] or α6 [54], were elevated, respectively. The expression of ICAM-1 was shown to be regulated by the actomyosin contractility of fibroblasts via ROCK-1 signaling [55]. Consistent with this, in the present study we have demonstrated that on softer dECM, MSCs displayed reduced ICAM-1 expression and *ROCK1* downregulation.

Spatial-mechanical regulation of cellular phenotype is characterized by bidirectional interactions. Here we have detected the upregulation of protease-encoding genes, such as *MMP1* and *PLAU*, in MSCs on dECM, which can reflect the activation of MSC-mediated ECM remodeling during recellularization [56]. In turn, physical forces transmitted via the ECM have been shown to directly activate nuclear transcription regulators, thereby influencing cell fate [57,58]. The identification of the transcriptional YAP and TAZ co-activators as key mechanosensors has provided significant insights into the understanding of how physical and mechanical signals from the ECM are translated into intracellular biochemical responses [59]. The described decrease in the nuclear-to-cytoplasmic YAP/TAZ ratio in recellularized MSCs is consistent with previous findings showing that increased substrate stiffness results in an increased nuclear–cytoplasmic YAP/TAZ ratio in MSCs [60]. In the nucleus, they are known to activate genes that support increased cytoskeletal tension via indirect mechanisms, including the assembly of stress fibers [61]. In contrast, a soft matrix with less organized fibrillar architecture is unable to generate anisotropic cytoskeletal tension [62], resulting in the retention of YAP/TAZ in the cytoplasm and their subsequent phosphorylation and degradation [60].

A principal finding of the present study is that YAP and TAZ, despite their structural homology, may perform distinct functions and can be differentially involved in MSC responses to dECM generated under physiological hypoxia or normoxia. We have found that the increased rigidity and alignment of the fibrils in the hypoxic ECM (5-dECM) generate a tension in the cytoskeleton along one axis that stabilizes YAP. At the same time, a preferential nuclear accumulation of TAZ was observed in MSCs on 20-dECM relative to 5-dECM. In recent studies, TAZ was shown to play a pivotal role in osteogenic lineage commitment in MSCs [63,64]. TAZ physically interacts with

the key osteogenic transcription factor Runx2, enhancing its transcriptional activity. Our findings provide a potential mechanistic explanation for the previously reported stimulatory effects of 20-dECM on MSC osteogenic differentiation, including increased *RUNX2* expression, elevated alkaline phosphatase activity, and enhanced production of osteogenesis-regulating cytokines [31]. Thus, our results suggest that oxygen levels during ECM production may determine the preferentially engaged mechanotransducer, which in turn might affect MSC fate through distinct YAP- or TAZ-dependent pathways.

It was demonstrated previously, application of dECM in cell culture protocols promotes various processes like proliferation, colony-forming ability, and differentiation [7,65,66]. In support, here we demonstrated that the enhanced MSC growth reduced intracellular ROS on both 20-dECM and 5-dECM compared with plastic, consistent with known antioxidant effects of dECM [5,7]. These benefits may arise from the complex proteomic composition of dECM, which retains structural proteins, matricellular glycoproteins, and growth factors that modulate cell behavior [67]. While bioinformatic and proteomic analyses can predict ECM-driven signaling pathways [68], the present study was not aimed at direct compositional characterization of the two substrates. Thus, whether the observed differences in the behavior of reseeded MSCs reflect biochemical versus mechanical/topographical cues remains unresolved. Future comparative proteomic and functional studies are needed to elucidate these mechanisms and guide the rational design of dECM scaffolds.

5. Limitation

Despite recent advances in cell-derived dECM, its translational application remains constrained by several factors. Its production is costly and labor-intensive, limiting scalability. Stringent quality control measures are required to ensure the complete removal of cellular and DNA contaminants, as even trace amounts of residual immunogenic material may elicit adverse host responses *in vivo*. Furthermore, the long-term stability of dECM materials remains a challenge, as both cryopreservation and lyophilization may compromise matrix integrity and bioactivity, necessitating further optimization of storage conditions. The establishment of clinical-grade manufacturing processes is further complicated by strict regulatory requirements, including the standardization of raw materials, batch-to-batch consistency, and comprehensive safety testing.

It should also be noted that all experiments were performed *in vitro* using human adipose-derived MSCs obtained from a limited number of donors. Primary cells inherently exhibit substantial donor-to-donor variability, which may affect the reproducibility of the findings. Furthermore, analysis of the YAP/TAZ signaling pathway in the present study was limited to assessment of nucleo-to-cytoplasmic translocation without detailed evaluation of downstream target gene expression, thereby precluding a comprehensive characterization of the functional activity of this mechanotransduction pathway. The functional implications of the observed alterations in YAP/TAZ localization in MSCs cultured on 20-dECM and 5-dECM therefore remain to be elucidated in future studies.

Finally, although 2D cultivation remains the most widely employed routine approach for investigating the effects of the microenvironment on ECM properties, it does not fully recapitulate the 3D architecture of native tissues, in which cells are embedded within a spatially organized ECM network that provides complex biochemical and biophysical cues. Consequently, validation of the present findings in physiologically relevant 3D culture systems will be an important direction for future research.

6. Conclusions

The presented data suggest that the local milieu of ECM-producing cells, the oxygen level in particular, plays a key role in determining the structural and mechanical properties of their ECM. The cultivation of MSCs under physiological hypoxia (5% O_2) was associated with the formation of ECM with pronounced fiber anisotropy and increased stiffness.

In comparison with uncoated plastic surfaces, dECM acted not only as structural support but also as an active regulator of cellular functions, ensuring efficient adhesion and mechanical coupling with cells. Regardless of oxygen conditions, dECM supported physiologically relevant phenotypes of recellularized MSCs, optimized adhesive interactions, reduced oxidative stress, and stimulated proliferative activity. Furthermore, the mechanical and topographical properties of dECM produced under different O_2 levels were correlated with the subcellular distribution of YAP and TAZ in recellularized MSCs. However, a direct link between dECM properties and the YAP/TAZ-dependent mechanotransduction pathways triggered remains to be established in future targeted studies.

These findings highlight the potential utility of dECM in regenerative medicine, both for the development of tissue-engineered constructs and for the optimization of cell culture protocols aimed at enhancing therapeutic efficacy. Furthermore, modulation of cell culture conditions may enable the customization of ECM properties, thereby facilitating the development of biomimetic substrates with predefined characteristics. Nevertheless, the successful translation of these opportunities into clinical practice will depend on overcoming the aforementioned challenges, including issues related to scalability, immunogenicity, storage stability, and regulatory compliance. Future studies should address these challenges to enable a comprehensive evaluation of the therapeutic potential of cell-derived dECM.

Availability of Data and Materials

The datasets obtained during this study are available from the corresponding author upon reasonable request.

Author Contributions

DM, EA, LB designed the study. DM and AG developed the methodology, conducted the research, formal analysis and were responsible for data collection. EA managed the project administration and provided funding and supervision for the study. DM and AG prepared the visualizations; DM wrote the original manuscript; EA and LB analyzed and revised the final version. All authors read and approved the final version of the manuscript. All authors have participated sufficiently in the work and agreed to be accountable for all aspects of the work. All authors contributed to editorial changes in the manuscript.

Ethics Approval and Consent to Participate

All experimental protocols were approved by the Medical Bioethics Commission of IBMP RAS (protocol No. 690/MSC, 11/08/25). The study was conducted in accordance with the principles of the Declaration of Helsinki. Written informed consent was obtained from all donors prior to adipose tissue collection.

Acknowledgment

The authors thank Irina V. Ogneva and Nikolay S. Biryukov for technical support in conducting atomic force microscopy. We also thank the Center for Microscopic Methods, Bioline (Moscow), and the Shared Research Facility "Electron Microscopy" of the Department of Biology, Lomonosov Moscow State University, for providing access to microscopes.

Funding

This research was funded by the Russian Science Foundation, grant No. 23-15-00062.

Conflicts of Interest

The authors declare no conflicts of interest.

Declaration of AI and AI-Assisted Technologies in the Writing Process

During the preparation of this work, the authors used DeepL translator with AI platform in order to translate and check grammar. After using this tool, the authors reviewed and edited the content as needed and take full responsibility for the content of the publication.

Supplementary Material

Supplementary material associated with this article can be found, in the online version, at https://doi.org/10.31083/FBL52962.

References

[1] Caplan AI, Correa D. The MSC: an injury drugstore. Cell Stem Cell. 2011; 9: 11–15. https://doi.org/10.1016/j.stem.2011.06.008

[2] Sagaradze GD, Basalova NA, Efimenko AY, Tkachuk VA. Mesenchymal Stromal Cells as Critical Contributors to Tissue Regeneration. Frontiers in Cell and Developmental Biology. 2020; 8: 576176. https://doi.org/10.3389/fcell.2020.576176

[3] Han X, Liao R, Li X, Zhang C, Huo S, Qin L, et al. Mesenchymal stem cells in treating human diseases: molecular mechanisms and clinical studies. Signal Transduction and Targeted Therapy. 2025; 10: 262. https://doi.org/10.1038/s41392-025-02313-9

[4] L PK, Kandoi S, Misra R, S V, K R, Verma RS. The mesenchymal stem cell secretome: A new paradigm towards cell-free therapeutic mode in regenerative medicine. Cytokine & Growth Factor Reviews. 2019; 46: 1–9. https://doi.org/10.1016/j.cytogfr.2019.04.002

[5] Pei M, He F, Kish VL. Expansion on extracellular matrix deposited by human bone marrow stromal cells facilitates stem cell proliferation and tissue-specific lineage potential. Tissue Engineering. Part a. 2011; 17: 3067–3076. https://doi.org/10.1089/ten.TEA.2011.0158

[6] Lin H, Yang G, Tan J, Tuan RS. Influence of decellularized matrix derived from human mesenchymal stem cells on their proliferation, migration and multi-lineage differentiation potential. Biomaterials. 2012; 33: 4480–4489. https://doi.org/10.1016/j.biomaterials.2012.03.012

[7] Liu X, Zhou L, Chen X, Liu T, Pan G, Cui W, et al. Culturing on decellularized extracellular matrix enhances antioxidant properties of human umbilical cord-derived mesenchymal stem cells. Materials Science & Engineering. C, Materials for Biological Applications. 2016; 61: 437–448. https://doi.org/10.1016/j.msec.2015.12.090

[8] Zhang W, Yang J, Zhu Y, Sun X, Guo W, Liu X, et al. Extracellular matrix derived by human umbilical cord-deposited mesenchymal stem cells accelerates chondrocyte proliferation and differentiation potential in vitro. Cell and Tissue Banking. 2019; 20: 351–365. https://doi.org/10.1007/s10561-019-09774-7

[9] Ushakov R, Ratushnyy A, Buravkova L, Tolkunova E, Burova E. The Decellularized Cell-Derived Extracellular Matrix Enhances the Paracrine Function of Human Mesenchymal Stromal/Stem Cells. International Journal of Molecular Sciences. 2024; 25: 2419. https://doi.org/10.3390/ijms25042419

[10] Prewitz MC, Seib FP, von Bonin M, Friedrichs J, Stißel A, Niehage C, et al. Tightly anchored tissue-mimetic matrices as instructive stem cell microenvironments. Nature Methods. 2013; 10: 788–794. https://doi.org/10.1038/nmeth.2523

[11] Hoshiba T, Sugano Y, Yokoyama N. Murine neural stem cell (NSC) line, MEB5-derived decellularized matrix as an in vitro extracellular matrix model in NSC niche. Chemistry Letters. 2018; 47: 1498–1501. https://doi.org/10.1246/cl.180788

[12] Gao CY, Huang ZH, Jing W, Wei PF, Jin L, Zhang XH, et al. Directing osteogenic differentiation of BMSCs by cell-secreted decellularized extracellular matrixes from different cell types. Journal of Materials Chemistry. B. 2018; 6: 7471–7485. https://doi.org/10.1039/c8tb01785a

[13] Guneta V, Zhou Z, Tan NS, Sugii S, Wong MTC, Choong C. Recellularization of decellularized adipose tissue-derived stem cells: role of the cell-secreted extracellular matrix in cellular differentiation. Biomaterials Science. 2017; 6: 168–178. https://doi.org/10.1039/c7bm00695k

[14] Anderson AE, Wu I, Parrillo AJ, Wolf MT, Maestas DR, Jr, Graham I, et al. An immunologically active, adipose-derived extracellular matrix biomaterial for soft tissue reconstruction: con-

cept to clinical trial. NPJ Regenerative Medicine. 2022; 7: 6. https://doi.org/10.1038/s41536-021-00197-1

[15] Noronha NDC, Mizukami A, Caliári-Oliveira C, Cominal JG, Rocha JLM, Covas DT, et al. Priming approaches to improve the efficacy of mesenchymal stromal cell-based therapies. Stem Cell Research & Therapy. 2019; 10: 131. https://doi.org/10.1186/s13287-019-1224-y

[16] Li M, Jiang Y, Hou Q, Zhao Y, Zhong L, Fu X. Potential pre-activation strategies for improving therapeutic efficacy of mesenchymal stem cells: current status and future prospects. Stem Cell Research & Therapy. 2022; 13: 146. https://doi.org/10.1186/s13287-022-02822-2

[17] Zhuo H, Chen Y, Zhao G. Advances in application of hypoxia-preconditioned mesenchymal stem cell-derived exosomes. Frontiers in Cell and Developmental Biology. 2024; 12: 1446050. https://doi.org/10.3389/fcell.2024.1446050

[18] Le B, Cressman A, Morales D, Fierro FA. First clinical experiences using preconditioning approaches to improve MSC-based therapies. Current Stem Cell Reports. 2024; 10: 1–7. https://doi.org/10.1007/s40778-023-00232-5

[19] Andreeva E, Zhidkova O, Matveeva D, Gornostaeva A, Lobanova M, Buravkova L. Ex Vivo Preconditioning as a Useful Tool for Modification of the Extracellular Matrix of Multipotent Mesenchymal Stromal Cells. International Journal of Molecular Sciences. 2025; 26: 6301. https://doi.org/10.3390/ijms26136301

[20] Ivanovic Z. Hypoxia or in situ normoxia: The stem cell paradigm. Journal of Cellular Physiology. 2009; 219: 271–275. https://doi.org/10.1002/jcp.21690

[21] Carreau A, El Hafny-Rahbi B, Matejuk A, Grillon C, Kieda C. Why is the partial oxygen pressure of human tissues a crucial parameter? Small molecules and hypoxia. Journal of Cellular and Molecular Medicine. 2011; 15: 1239–1253. https://doi.org/10.1111/j.1582-4934.2011.01258.x

[22] Morikawa T, Takubo K. Hypoxia regulates the hematopoietic stem cell niche. Pflugers Archiv: European Journal of Physiology. 2016; 468: 13–22. https://doi.org/10.1007/s00424-015-1743-z

[23] Mas-Bargues C, Sanz-Ros J, Román-Domínguez A, Inglés M, Gimeno-Mallench L, El Alami M, et al. Relevance of Oxygen Concentration in Stem Cell Culture for Regenerative Medicine. International Journal of Molecular Sciences. 2019; 20: 1195. https://doi.org/10.3390/ijms20051195

[24] da Graça Cabreira M, Wang X, Critsinelis A, Setegne M, Lotfi P, Wan YW, et al. Environmental oxygen affects ex vivo growth and proliferation of mesenchymal progenitors by modulating mitogen-activated protein kinase and mammalian target of rapamycin signaling. Cytotherapy. 2022; 24: 1201–1210. https://doi.org/10.1016/j.jcyt.2022.06.005

[25] Volkova MV, Shen N, Polyanskaya A, Qi X, Boyarintsev VV, Kovaleva EV, et al. Tissue-Oxygen-Adaptation of Bone Marrow-Derived Mesenchymal Stromal Cells Enhances Their Immunomodulatory and Pro-Angiogenic Capacity, Resulting in Accelerated Healing of Chemical Burns. International Journal of Molecular Sciences. 2023; 24: 4102. https://doi.org/10.3390/ijms24044102

[26] Beegle J, Lakatos K, Kalomoiris S, Stewart H, Isseroff RR, Nolta JA, et al. Hypoxic preconditioning of mesenchymal stromal cells induces metabolic changes, enhances survival, and promotes cell retention in vivo. Stem Cells (Dayton, Ohio). 2015; 33: 1818–1828. https://doi.org/10.1002/stem.1976

[27] Ishiuchi N, Nakashima A, Doi S, Yoshida K, Maeda S, Kanai R, et al. Hypoxia-preconditioned mesenchymal stem cells prevent renal fibrosis and inflammation in ischemia-reperfusion rats. Stem Cell Research & Therapy. 2020; 11: 130. https://doi.org/10.1186/s13287-020-01642-6

[28] Yang Y, Wu Y, Yang D, Neo SH, Kadir ND, Goh D, et al. Secretive derived from hypoxia preconditioned mesenchymal stem cells promote cartilage regeneration and mitigate joint inflammation via extracellular vesicles. Bioactive Materials. 2023; 27: 98–112. https://doi.org/10.1016/j.bioactmat.2023.03.017

[29] Deschene K, Céleste C, Boerboom D, Theoret CL. Hypoxia regulates the expression of extracellular matrix associated proteins in equine dermal fibroblasts via HIF1. Journal of Dermatological Science. 2012; 65: 12–18. https://doi.org/10.1016/j.jdermsci.2011.09.006

[30] Gornostaeva A, Buravkova L, Lobanova M, Andreeva E. HIFs in hypoxic regulation of the extracellular matrix: focus on little-known player HIF-3. BIOCELL. 2024; 48: 677–692. https://doi.org/10.32604/biocell.2024.048873

[31] Matveeva D, Buravkov S, Andreeva E, Buravkova L. Hypoxic Extracellular Matrix Preserves Its Competence after Expansion of Human MSCs under Physiological Hypoxia In Vitro. Biomimetics (Basel, Switzerland). 2023; 8: 476. https://doi.org/10.3390/biomimetics8060476

[32] Feng K, Yu Y, Chen Z, Wang F, Zhang K, Chen H, et al. Injectable hypoxia-preconditioned cartilage progenitor cells-laden GelMA microspheres system for enhanced osteoarthritis treatment. Materials Today. Bio. 2023; 20: 100637. https://doi.org/10.1016/j.mtbio.2023.100637

[33] Makris EA, Hu JC, Athanasiou KA. Hypoxia-induced collagen crosslinking as a mechanism for enhancing mechanical properties of engineered articular cartilage. Osteoarthritis and Cartilage. 2013; 21: 634–641. https://doi.org/10.1016/j.joca.2013.01.007

[34] Dominici M, Le Blanc K, Mueller I, Slaper-Cortenbach I, Marini F, Krause D, et al. Minimal criteria for defining multipotent mesenchymal stromal cells. The International Society for Cellular Therapy position statement. Cytotherapy. 2006; 8: 315–317. https://doi.org/10.1080/14653240600855905

[35] Maia FR, Reis RL, Oliveira JM. Decellularized hASCs-derived matrices as biomaterials for 3D in vitro approaches. Methods in Cell Biology. 2020; 156: 45–58. https://doi.org/10.1016/bs.mcb.2019.11.019

[36] Golebiowska AA, Intravaia JT, Sathe VM, Kumbar SG, Nukavarapu SP. Decellularized extracellular matrix biomaterials for regenerative therapies: Advances, challenges and clinical prospects. Bioactive Materials. 2024; 32: 98–123. https://doi.org/10.1016/j.bioactmat.2023.09.017

[37] Harris GM, Raitman I, Schwarzbauer JE. Cell-derived decellularized extracellular matrices. Methods in Cell Biology. 2018; 143: 97–114. https://doi.org/10.1016/bs.mcb.2017.08.007

[38] Du HC, Jiang L, Geng WX, Li J, Zhang R, Dang JG, et al. Evaluation of xenogeneic extracellular matrix fabricated from $CuCl_2$-conditioned mesenchymal stem cell sheets as a bioactive wound dressing material. Journal of Biomaterials Applications. 2017; 32: 472–483. https://doi.org/10.1177/0885328217731951

[39] Braga CL, da Silva LR, Santos RT, de Carvalho LRP, Mandacaru SC, de Oliveira Trugilho MR, et al. Proteomics profile of mesenchymal stromal cells and extracellular vesicles in normoxic and hypoxic conditions. Cytotherapy. 2022; 24: 1211–1224. https://doi.org/10.1016/j.jcyt.2022.08.009

[40] Matveeva D, Andreeva E, Rudimova Y, Gornostaeva A, Yakubets D, Andrianova I, et al. Alterations of matrisome gene expression in multipotent mesenchymal stromal cells under physiological hypoxia in vitro. Tissue & Cell. 2025; 97: 103064. https://doi.org/10.1016/j.tice.2025.103064

[41] Kusuma GD, Brennecke SP, O'Connor AJ, Kalionis B, Heath DE. Decellularized extracellular matrices produced from immortal cell lines derived from different parts of the placenta support primary mesenchymal stem cell expansion. PloS One. 2017; 12: e0171488. https://doi.org/10.1371/journal.pone.0171488

[42] Jean C, Gravelle P, Fournie JJ, Laurent G. Influence of stress on extracellular matrix and integrin biology. Oncogene. 2011; 30: 2697–2706. https://doi.org/10.1038/onc.2011.27
[43] Riis S, Stensballe A, Emmersen J, Pennisi CP, Birkelund S, Zachar V, et al. Mass spectrometry analysis of adipose-derived stem cells reveals a significant effect of hypoxia on pathways regulating extracellular matrix. Stem Cell Research & Therapy. 2016; 7: 52. https://doi.org/10.1186/s13287-016-0310-7
[44] Wobma HM, Kanai M, Ma SP, Shih Y, Li HW, Duran-Struuck R, et al. Dual IFN-γ/hypoxia priming enhances immunosuppression of mesenchymal stromal cells through regulatory proteins and metabolic mechanisms. Journal of Immunology and Regenerative Medicine. 2018; 1: 45–56. https://doi.org/10.1016/j.regen.2018.01.001
[45] Geiger B, Yamada KM. Molecular architecture and function of matrix adhesions. Cold Spring Harbor Perspectives in Biology. 2011; 3: a005033. https://doi.org/10.1101/cshperspect.a005033
[46] Wang WY, Pearson AT, Kutys ML, Choi CK, Wozniak MA, Baker BM, et al. Extracellular matrix alignment dictates the organization of focal adhesions and directs uniaxial cell migration. APL Bioengineering. 2018; 2: 046107. https://doi.org/10.1063/1.5052239
[47] Harris GM, Madigan NN, Lancaster KZ, Enquist LW, Windebank AJ, Schwartz J, et al. Nerve Guidance by a Decellularized Fibroblast Extracellular Matrix. Matrix Biology: Journal of the International Society for Matrix Biology. 2017; 60-61: 176–189. https://doi.org/10.1016/j.matbio.2016.08.011
[48] Bauer AL, Jackson TL, Jiang Y. Topography of extracellular matrix mediates vascular morphogenesis and migration speeds in angiogenesis. PLoS Computational Biology. 2009; 5: e1000445. https://doi.org/10.1371/journal.pcbi.1000445
[49] Yang L, Ge L, van Rijn P. Synergistic Effect of Cell-Derived Extracellular Matrices and Topography on Osteogenesis of Mesenchymal Stem Cells. ACS Applied Materials & Interfaces. 2020; 12: 25591–25603. https://doi.org/10.1021/acsami.0c05012
[50] Jia S, Liu L, Pan W, Meng G, Duan C, Zhang L, et al. Oriented cartilage extracellular matrix-derived scaffold for cartilage tissue engineering. Journal of Bioscience and Bioengineering. 2012; 113: 647–653. https://doi.org/10.1016/j.jbiosc.2011.12.009
[51] Chastney MR, Conway JRW, Ivaska J. Integrin adhesion complexes. Current Biology: CB. 2021; 31: R536–R542. https://doi.org/10.1016/j.cub.2021.01.038
[52] Riveline D, Zamir E, Balaban NQ, Schwarz US, Ishizaki T, Narumiya S, et al. Focal contacts as mechanosensors: externally applied local mechanical force induces growth of focal contacts by an mDia1-dependent and ROCK-independent mechanism. The Journal of Cell Biology. 2001; 153: 1175–1186. https://doi.org/10.1083/jcb.153.6.1175
[53] McCall-Culbreath KD, Zutter MM. Collagen receptor integrins: rising to the challenge. Current Drug Targets. 2008; 9: 139–149. https://doi.org/10.2174/138945008783502494
[54] Marchetti G, De Arcangelis A, Pfister V, Georges-Labouesse E. α6 integrin subunit regulates cerebellar development. Cell Adhesion & Migration. 2013; 7: 325–332. https://doi.org/10.4161/cam.25140
[55] Bonan S, Albrengues J, Grasset E, Kuzet SE, Nottet N, Bourget I, et al. Membrane-bound ICAM-1 contributes to the onset of proinvasive tumor stroma by controlling acto-myosin contractility in carcinoma-associated fibroblasts. Oncotarget. 2017; 8: 1304–1320. https://doi.org/10.18632/oncotarget.13610
[56] Ramanathan A, Karuri N. Proteolysis of decellularized extracellular matrices results in loss of fibronectin and cell binding activity. Biochemical and Biophysical Research Communications. 2015; 459: 246–251. https://doi.org/10.1016/j.bbrc.2015.02.092
[57] Muncie JM, Weaver VM. The Physical and Biochemical Properties of the Extracellular Matrix Regulate Cell Fate. Current Topics in Developmental Biology. 2018; 130: 1–37. https://doi.org/10.1016/bs.ctdb.2018.02.002
[58] Wang T, Nanda SS, Papaefthymiou GC, Yi DK. Mechanophysical Cues in Extracellular Matrix Regulation of Cell Behavior. Chembiochem: a European Journal of Chemical Biology. 2020; 21: 1254–1264. https://doi.org/10.1002/cbic.201900686
[59] Panciera T, Azzolin L, Cordenonsi M, Piccolo S. Mechanobiology of YAP and TAZ in physiology and disease. Nature Reviews. Molecular Cell Biology. 2017; 18: 758–770. https://doi.org/10.1038/nrm.2017.87
[60] Caliari SR, Vega SL, Kwon M, Soulas EM, Burdick JA. Dimensionality and spreading influence MSC YAP/TAZ signaling in hydrogel environments. Biomaterials. 2016; 103: 314–323. https://doi.org/10.1016/j.biomaterials.2016.06.061
[61] Jafarinia H, Khalilimeybodi A, Barrasa-Fano J, Fraley SI, Rangamani P, Carlier A. Insights gained from computational modeling of YAP/TAZ signaling for cellular mechanotransduction. NPJ Systems Biology and Applications. 2024; 10: 90. https://doi.org/10.1038/s41540-024-00414-9
[62] Scott KE, Fraley SI, Rangamani P. A spatial model of YAP/TAZ signaling reveals how stiffness, dimensionality, and shape contribute to emergent outcomes. Proceedings of the National Academy of Sciences of the United States of America. 2021; 118: e2021571118. https://doi.org/10.1073/pnas.2021571118
[63] Zhu Y, Wu Y, Cheng J, Wang Q, Li Z, Wang Y, et al. Pharmacological activation of TAZ enhances osteogenic differentiation and bone formation of adipose-derived stem cells. Stem Cell Research & Therapy. 2018; 9: 53. https://doi.org/10.1186/s13287-018-0799-z
[64] Zhao X, Tang L, Le TP, Nguyen BH, Chen W, Zheng M, et al. Yap and Taz promote osteogenesis and prevent chondrogenesis in neural crest cells in vitro and in vivo. Science Signaling. 2022; 15: eabn9009. https://doi.org/10.1126/scisignal.abn9009
[65] Rakian R, Block TJ, Johnson SM, Marinkovic M, Wu J, Dai Q, et al. Native extracellular matrix preserves mesenchymal stem cell “stemness” and differentiation potential under serum-free culture conditions. Stem Cell Research & Therapy. 2015; 6: 235. https://doi.org/10.1186/s13287-015-0235-6
[66] Van SY, Noh YK, Kim SW, Oh YM, Kim IH, Park K. Human umbilical cord blood mesenchymal stem cells expansion via human fibroblast-derived matrix and their potentials toward regenerative application. Cell and Tissue Research. 2019; 376: 233–245. https://doi.org/10.1007/s00441-018-2971-2
[67] Ragelle H, Naba A, Larson BL, Zhou F, Prijić M, Whittaker CA, et al. Comprehensive proteomic characterization of stem cell-derived extracellular matrices. Biomaterials. 2017; 128: 147–159. https://doi.org/10.1016/j.biomaterials.2017.03.008
[68] Novoseletskaya ES, Evdokimov PV, Efimenko AY. Extracellular matrix-induced signaling pathways in mesenchymal stem/stromal cells. Cell Communication and Signaling: CCS. 2023; 21: 244. https://doi.org/10.1186/s12964-023-01252-8